ChemPubSoc Europe

DOI: 10.1002/cssc.201902394

CHEMSUSCHEM Full Papers

Flexible Freestanding MoO_{3-x}–Carbon Nanotubes–Nanocellulose Paper Electrodes for Charge-Storage Applications

Ahmed S. Etman,*[a, c] Zhaohui Wang,*[b] Ahmed El Ghazaly,[a] Junliang Sun,[d] Leif Nyholm,[b] and Johanna Rosen*[a]

Herein, a one-step synthesis protocol was developed for synthesizing freestanding/flexible paper electrodes composed of nanostructured molybdenum oxide (MoO_{3-x}) embedded in a carbon nanotube (CNT) and *Cladophora* cellulose (CC) matrix. The preparation method involved sonication of the precursors, nanostructured MoO_{3-x}, CNTs, and CC with weight ratios of 7:2:1, in a water/ethanol mixture, followed by vacuum filtration. The electrodes were straightforward to handle and possessed a thickness of approximately 12 μm and a mass loading of MoO_{3-x}–CNTs of approximately 0.9 mg cm^{-2}. The elemental mapping showed that the nanostructured MoO_{3-x} was uniformly embedded inside the CNTs–CC matrix. The MoO_{3-x}–CNTs–CC paper electrodes featured a capacity of 30 C g^{-1}, normalized to the mass of MoO_{3-x}–CNTs, at a current density of 78 A g^{-1} (corresponding to a rate of approximately 210 C based on the MoO_3 content, assuming a theoretical capacity of 1339 C g^{-1}), and exhibited a capacity retention of 91% over 30 000 cycles. This study paves the way for the manufacturing of flexible/freestanding nanostructured MoO_{3-x}-based electrodes for use in charge-storage devices at high charge/discharge rates.

Introduction

Nowadays, charge-storage devices are widely used in many applications including portable devices, wearable electronics, and electric vehicles.[1–3] These applications require the electrode materials to be lightweight, and to exhibit high flexibilities and good high-rate performances so that the electrodes can be charged rapidly. In general, electrochemical charge-storage devices can store charge based on two different mechanisms. The first mechanism involves storing the charge at the electrode/electrolyte interfaces in electrochemical double-layer capacitors (EDLCs).[4] These EDLCs typically employ carbonaceous electrode materials with high surface areas[5,6] because the charge-storing capacities depend on the electrochemically active area of these electrodes. The second mechanism, in which the charge storage results from electrochemical reactions involving the electrode materials, can involve a range of materials such as electronically conductive polymers and transition-metal oxides.[7–10] Compared with the carbonaceous electrodes, the electrochemically active electrodes generally exhibit higher energy densities but also often require lower charge and discharge rates as a result of the fact that the entire volume of the electrode then can be employed (compared with only the electrode surface in the double-layer capacitance case). Many researchers have therefore focused on the preparation of hybrid electrode materials, composed of thin layers of electroactive materials coated on substrates with large surface areas, to obtain high capacities as well as high charge and discharge rate capabilities.[10,11]

Cellulose is a sustainable and biodegradable material, as well as the most abundant natural polymer, and it can be extracted from wood, algae, and bacteria.[10,12–16] Cellulose can be used in many applications, including water purification, fire-retardants, and paper manufacturing.[13,14] In the last few years, nanocellulose has been used to fabricate paper-based flexible electrodes for energy-storage applications, owing to its resource abundance, high mechanical flexibility, and excellent solution processability.[10,16–22] Although many methods have been used to prepare paper-based electrodes, including printing methods, vaporization methods, and vacuum-filtration methods,[17,22] Wang et al.[23,24] recently introduced a robust

[a] Dr. A. S. Etman, A. El Ghazaly, Prof. J. Rosen
Department of Physics, Chemistry and Biology (IFM)
Linköping University
58183, Linköping (Sweden)
E-mail: ahmed.etman@liu.se
johanna.rosen@liu.se

[b] Dr. Z. Wang, Prof. L. Nyholm
Department of Chemistry, Ångström Laboratory
Uppsala University
75121 Uppsala (Sweden)
E-mail: zhaohui.wang@kemi.uu.se

[c] Dr. A. S. Etman
Department of Chemistry
Faculty of Science
Alexandria University
Ibrahimia, Alexandria 21321 (Egypt)

[d] Prof. J. Sun
College of Chemistry and Molecular Engineering
Peking University
Yiheyuan Road 5, Beijing 100871 (P.R. China)

Supporting Information and the ORCID identification number(s) for the author(s) of this article can be found under: https://doi.org/10.1002/cssc.201902394.

synthesis protocol for the manufacturing of flexible freestanding paper electrodes by using a combination of a redox-active material, carbon nanotubes (CNTs), and *Cladophora* cellulose (CC). Therefore, there is a need to explore the extension of the aforementioned synthesis approach to include some other redox-active materials such as transition-metal oxide nanosheets (e.g., vanadium[25–27] or molybdenum oxide nanosheets).[28,29]

Molybdenum oxides have previously been used in a variety of electrochemical applications such as electrode materials for lithium-ion batteries, sodium-ion batteries, and supercapacitors.[30–35] However, molybdenum oxide-based electrodes usually suffer from low electronic conductivities, fast capacity fading, and poor electrochemical cyclabilities.[36] So far, many modifications have been described in literature to improve the performance of molybdenum oxide-based electrodes; for example, some studies have shown that the use of reduced molybdenum oxides (MoO_{3-x}) rather than MoO_3 can increase the pseudocapacitance of electrodes.[37] In addition, the inclusion of conductive additives such as graphene[11] or CNTs[34,38] has been shown to enhance the electrochemical behavior of molybdenum oxide electrodes. The conventional electrode fabrication method commonly involves the use of organic binder, which can influence the electrochemical behavior of the electrodes, for example, by reducing the accessible capacity and long-term cycling stability.[38] Recently, Huang et al.[39] and Yao et al.[35] reported synthesis protocols for fabricating freestanding MoO_3 nanopapers to overcome on the use of organic binder. Likewise, freestanding electrodes were also fabricated by drop casting a dispersion of molybdenum oxide onto a conductive substrate.[28]

Recently, we reported the use of freestanding electrodes of reduced MoO_{3-x} nanosheets deposited onto carbon paper for charge-storage applications,[28,40] which showed good electrochemical performance when used in electrodes in which the thickness of the active material was limited to approximately 4–5 μm. The limited thickness of the active material meant that the capacities of the electrodes were relatively low, and because the electrodes also could be cycled for only approximately 2000 cycles, it was immediately clear that another electrode manufacturing approach would be required to allow this type of electrodes be used in energy-storage devices, that is, a method that enables the increase of the active material thickness and stabilizes the long-term cycling. One approach to increase the performance of these electrodes could be to mix the molybdenum trioxide with a conductive additive such as a carbonaceous material (e.g., graphene or CNTs),[32,33,41] and nanocellulose to yield flexible and freestanding paper electrodes by using the approach recently employed to make conductive nanofiber networks composed of CNTs and nanocellulose.[23,24]

The present work describes a straightforward approach for the manufacturing of porous, freestanding, and flexible electrodes composed of MoO_{3-x}–CNTs–CC, in which the CC serves as a dispersing agent and flexible substrate, whereas the CNTs act as a conductive additive. The electrodes were tested in 1.0 M H_2SO_4 and cycled between 0 and 0.5 V vs. Ag/AgCl (1 M KCl). The mass of the electrodes was between 0.10 and 0.21 mg, and their lateral dimensions were approximately 2–3 mm. The capacity was normalized to the mass of MoO_{3-x}–CNTs, which corresponded to approximately 90% of the electrode mass.

Results and Discussion

Paper-based electrodes have recently attracted a lot of attention owing to their applicability in conjunction with wearable electronics. In this study, the MoO_{3-x}–CNTs–CC paper electrodes were prepared by using a straightforward one-step vacuum-filtration method. A mixture of MoO_{3-x} nanosheets (prepared by using a previously described water-based exfoliation technique),[28] CNTs, and CC in weight ratios of 7:2:1 was first dispersed in a 3:1 water/ethanol mixture, after which the suspension was filtrated under vacuum to yield a freestanding paper electrode. Figure 1a displays a schematic illustration of the fabrication of the MoO_{3-x}–CNTs–CC paper electrode. The detailed structural and morphological characterizations of the MoO_{3-x} precursor were described in a previous report.[28]

The XRD pattern of the obtained MoO_{3-x}–CNTs–CC paper (see Figure S1a in the Supporting Information) indicated that the material was close to amorphous and that the degree of the crystallinity of the MoO_{3-x} nanosheets was low, in good agreement with previous findings.[28,29] The peak observed at 14.5° can be assigned to the CNTs–CC matrix beause it was also observed in the XRD pattern of the CNTs–CC paper. Interestingly, the MoO_{3-x}–CNTs–CC paper electrodes featured an electronic conductivity of approximately 0.019 S cm^{-1}, as determined by using four-point probe measurements. This electronic conductivity value shows that the electrical properties of the

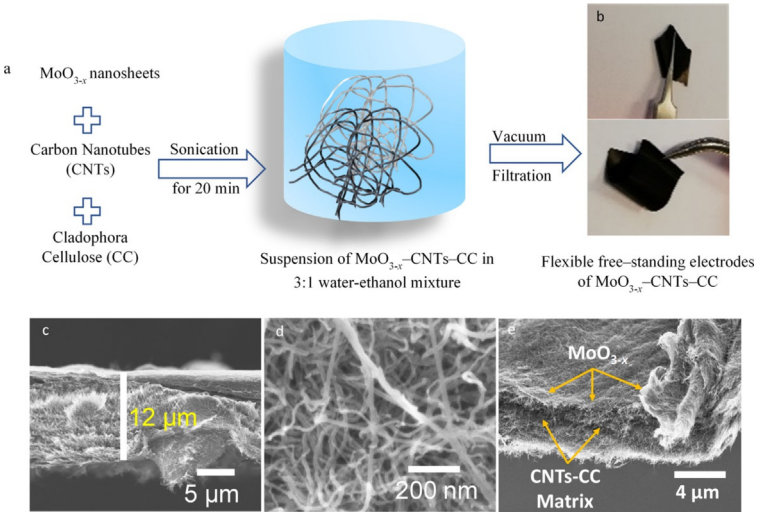

Figure 1. Synthesis and morphology of the MoO_{3-x}–CNTs–CC paper electrode. (a) Schematic illustration of the paper-electrode manufacturing process. (b) Photos of the paper electrodes showing their flexibility. (c, d) Low- and high-magnification SEM cross-section images, respectively, showing the thickness and homogeneity of the electrodes. (e) SEM top-view image, displaying the uniform distribution of MoO_{3-x} on the CNTs–CC matrix.

present MoO_{3-x}–CNTs–CC paper were comparable to those of previously described MoO_3-based nanopaper electrodes.[35,39] In addition, the MoO_{3-x}–CNTs–CC paper electrodes were highly flexible as shown in Figure 1b. The flexibility was confirmed by measurement of its Young's modulus by using nanoindentation tests, yielding a value of approximately (5.3 ± 0.6) GPa (see Figure S1 in the Supporting Information). The high flexibility of the paper electrodes reduces the internal strain inside the electrodes during the long-term electrochemical cycling.[16,42] It is worth noting that the flexibility of the here investigated electrodes is expected to be better than previous studies, in which the Young's modulus values were not clearly stated.[35,39]

Figure 1c shows a SEM cross-section image of the MoO_{3-x}–CNTs–CC paper, which had a thickness of approximately 12 μm. By using a high magnification (Figure 1d), it can be seen that the nanostructured MoO_{3-x} was uniformly distributed inside a matrix of randomly oriented CNTs–CC fibers. Likewise, the SEM top-view showed that the MoO_{3-x} is homogenously immobilized on the CNTs–CC matrix. Energy-dispersive X-ray (EDX) mapping also confirmed that the MoO_{3-x} was embedded inside the CNTs–CC matrix (see Figure S1 in the Supporting Information). It should be mentioned that it is challenging to distinguish between the CNT and CC fibers because they have very similar diameters.[24]

To study the electrochemical properties of the MoO_{3-x}–CNTs–CC paper, cyclic voltammetry (CV) experiments were performed between 0 and 0.5 V vs. Ag/AgCl (1 M KCl) in an electrolyte composed of 1.0 M H_2SO_4. The open-circuit potential (OCP) of the electrodes was approximately 0.25 V, and during the CV measurement the potential was swept from the OCP down to 0 V, after which the scan was reversed to 0.5 V, that is, the electrodes were first reduced and then oxidized. As seen in Figure 2a, the CVs obtained at a scan rate of 10 mV s^{-1} displayed two well-defined redox peaks, which can be assigned to the redox reactions of $Mo^{6+} \leftrightarrow Mo^{5+}$ and $Mo^{5+} \leftrightarrow Mo^{4+}$.[43,44] The redox peaks located at approximately 0.19 V (cathodic peak) and 0.21 V (anodic peak) thus stem from the Mo^{5+}/Mo^{4+} redox system, whereas the peaks observed at approximately 0.29 V (cathodic peak) and 0.31 V (anodic peak) can be ascribed to the reduction of Mo^{6+} and oxidation of Mo^{5+}, respectively. As can be seen in Figure 1a, the oxidation state of the molybdenum was mainly +5 in the as-prepared MoO_{3-x}–CNTs–CC paper electrode (because the OCP was 0.25 V, which is beyond the first reduction reaction of $Mo^{6+} \leftrightarrow Mo^{5+}$ occurring at potential of 0.29 V, and thus Mo^{5+} is the dominant oxidation state at the OCP). Interestingly, the shapes of the voltammograms did not change during the first few cycles, as can be seen in Figure 2a, in which the first (black), second (red), and eleventh (blue) cycles almost superimpose. This indicates that the electrochemical behavior of the MoO_{3-x}-based electrode was highly reversible. It is worth noting that previous reports have shown that the CNTs also are electrochemically active and thus contribute to the measured capacity.[24] In this study, the obtained capacity was therefore normalized by using the mass of both the MoO_{3-x} and CNTs, which correspond to approximately 90% of the electrode mass.

The shapes of the voltammograms in Figure 2b also maintained their symmetries upon increasing the scan rate from 10 to 20, 50, and 100 mV s^{-1}, indicating that the kinetics of the electrochemical reactions were fast (with a scan rate of 100 mV s^{-1}, the durations of the oxidation and reduction scans were merely 5 s). Moreover, the average capacity of approximately 30 C g^{-1} was almost independent of the scan rate, and the coulombic efficiency was close to 100% (see Figure 2c and Figure S2 in the Supporting Information). In addition, the long-term cycling at high (1000 mV s^{-1}), moderate (50 mV s^{-1}), and low (10 mV s^{-1}) cycling rates showed a stable electrochemical behavior over approximately 10000 cycles (see Figure S2 in the Supporting Information). This high rate performance reflects the fast kinetics of the redox reactions mentioned above. The contribution of the CNTs to the measured capacity was evaluated by testing CNTs–CC electrodes with a weight ratio of 1:1, and the discharge profiles showed that the CNT capacities were approximately 22 and 16 C g^{-1} when using current densities of 1 and 70 A g^{-1}, respectively (see Figure S2d,e in the Supporting Information). Provided that the CNT content in the MoO_{3-x}-CNTs-CC electrodes was approximately 20%, the CNTs would hence give rise to a contribution of approximately 3.3–4.5 C g^{-1}, that is, 11–15% of the measured capacity (see Table S1 in the Supporting Information).

It is worth noting that the specific capacity of the electrodes was quite low (30 C g^{-1}), even though the capacity would increase slightly to approximately 40 C g^{-1} upon normalization with respect to the MoO_{3-x} mass only (70% of overall electrode mass). However, the capacity is still much lower than the theoretical capacity of approximately 1339 C g^{-1}; that is, the electroactive fraction of MoO_{3-x} is approximately 3%. This finding indicates that only the surface of the MoO_{3-x} layer immobilized on the CNTs-CC matrix was electroactive.[28] This hypothesis is also supported by the well-defined peak shape in CVs seen at the different scan rates, which indicates that the redox reactions were surface-confined and not diffusion-controlled. Figure 2g shows a schematic illustration of the MoO_{3-x} immobilized onto the CNTs–CC fiber, for which it was assumed that only the surface MoO_{3-x} layer was electroactive. Because this and the low mass loading (0.19 mg) resulted in a capacity of the electrodes of approximately 5.6×10^{-3} C, it is clear that the capacities of the present type of electrode, as well as many other electrodes described in the literature, are not well optimized for being used directly in high-capacity devices. Therefore, further research studies should be focused on developing electrodes with significantly higher mass loadings in which all the electroactive material can be readily accessed. One possible solution to increase the capacity of the MoO_{3-x}–CNTs–CC paper electrode could be to increase the lateral size of the MoO_{3-x} flakes as previously shown by Coleman and co-workers.[34]

The reversibility of the system was estimated from the variation of the peak-to-peak separation (ΔU_p) between the reduction and oxidation peaks (i.e., between peak 1 and 1′, and between peak 2 and 2′, respectively) as a function of the scan rate.[28,44] As seen in Figure 2d, ΔU_p remained lower than 50 mV at the different scan rates. The linear increase in the

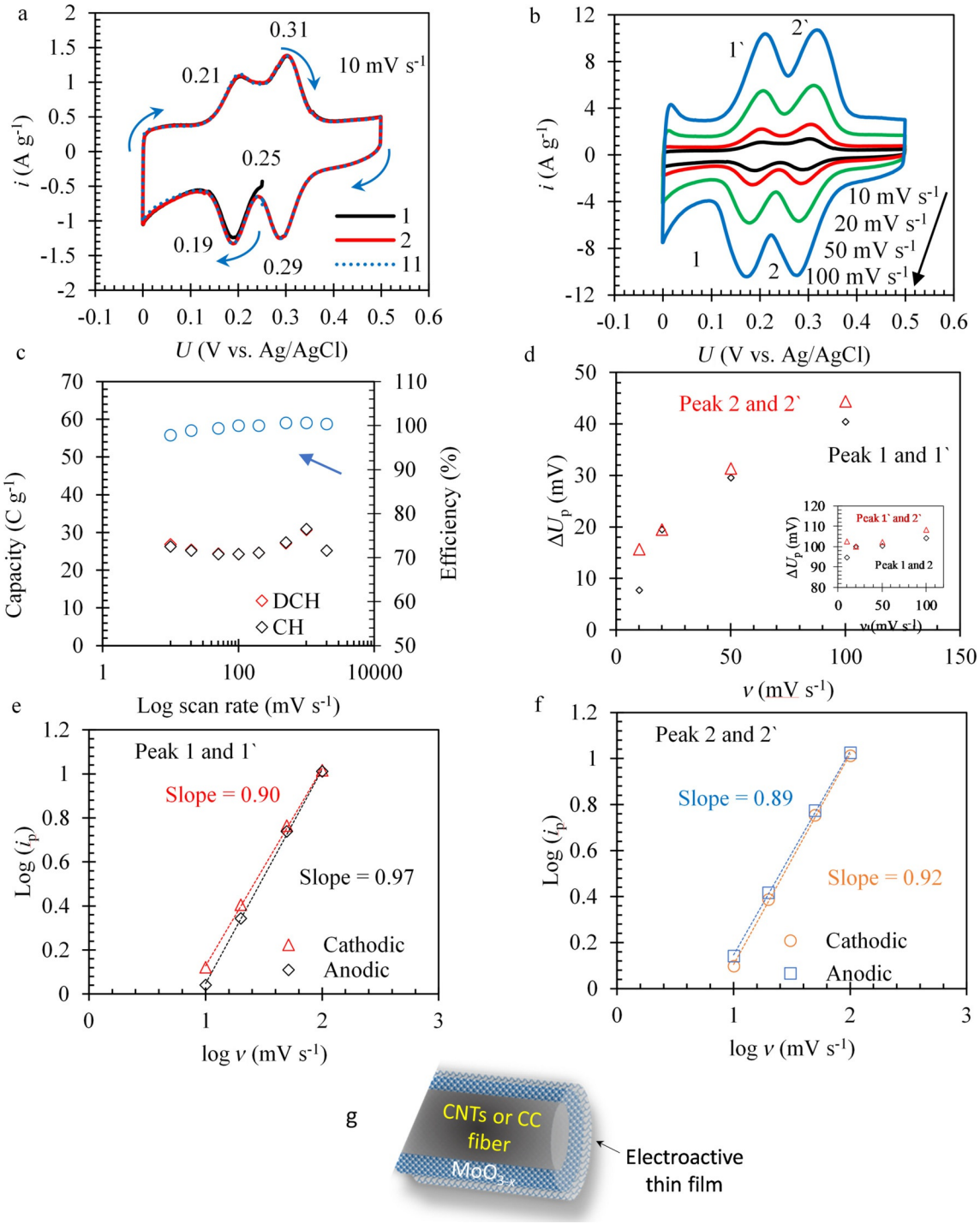

Figure 2. Study of the electrochemical performance of the MoO_{3-x}–CNTs–CC paper electrodes by CV. (a, b) Voltammograms recorded at a scan rate of 10 mV s^{-1} and different scan rates, respectively. The arrows in (a) indicate the scan direction. (c) Capacity and coulombic efficiency as a function of the scan rate. (d) Peak-to-peak separations (ΔU_p) as a function of the scan rate for redox peaks 1 and 1′ (black), and redox peaks 2 and 2′ (red). The inset displays the dependence of ΔU_p on the scan rate for the reduction–reduction (black) peaks and the oxidation–oxidation (red) peaks. (e, f) Logarithm of the peak current (i_p) as a function of the logarithm of the scan rate for peaks 1 and 1′, and peaks 2 and 2′, respectively. (g) Schematic illustration of MoO_{3-x} immobilized onto the CNTs–CC fiber, showing the thin electroactive layer of MoO_{3-x}.

peak-to-peak separation upon increasing the scan rate from 10 to 100 mV s^{-1} can mainly be attributed to *iR* (i.e., ohmic-drop) effects.[4,45] This observation is further supported by the fact that the peak-to-peak separations between peak 1 and 2, and between peak 1′ and 2′, respectively, were independent of the scan rate (inset in Figure 2d). A plot of the logarithm of the absolute value of the peak current as a function of the logarithm of the scan rate (Figure 2e, f) indicates that the redox reaction was surface-confined because the obtained slopes were very close to unity (0.89–0.97). This behavior further supports the

aforementioned hypothesis regarding the electroactivity of only the surface of the oxide layer deposited within the CNTs–CC matrix.

Constant-current charge and discharge curves were also recorded for the MoO_{3-x}–CNTs–CC paper electrodes. As can be seen in Figure 3a, the observed behavior was analogous to that seen in the CV experiments. Both the discharge (i.e., reduction) and charge (i.e., oxidation) curves thus featured two plateaus at approximately 0.29 and 0.19 V and 0.30 and 0.20 V, respectively, for an applied current density of 0.78 A g^{-1}. In Figure 3c, superimposed discharge profiles can be seen for current densities of 0.78 and 7.8 A g^{-1}, which are in good agreement with the high rate performance and *iR* drop discussed above. Furthermore, the capacity remained almost constant, and the coulombic efficiency stayed close to 100% upon increasing the current density up to 78 A g^{-1} as shown in Figure 3e and Figure S3 (in the Supporting Information). It worth mentioning that the applied currents were 100 μA and 10 mA at current densities of 0.78 and 78 A g^{-1}, respectively, owing to the relatively low amount of electroactive material. These low currents explain why the increase in the *iR* drop was relatively low when increasing the applied current density by an order of magnitude. The small increase in the *iR* drop combined with the fact that the redox reactions are surface-confined explain why the accessible capacities and the coulombic efficiency remained unchanged although the current density was increased by a factor of ten and the cut-off voltages remained the same (0 and 0.5 V for the lower and upper cut-off limits, respectively). These results hence clearly indicate that the magnitude of the *iR* drop and hence also the dependence of the capacity on the cycling rate is strongly dependent on the electroactive mass of the electrodes. For example, the discharge profiles for electrodes with larger sizes (5 mm × 7 mm) and mass loadings (total mass 320 μg) showed more pronounced *iR* drops and a decrease in the electrode capacity (see Figure S3c in the Supporting Information), especially at high current density of 70 mA g^{-1} (corresponding to approximately 20 mA absolute current). Care should therefore be taken when comparing rate performances of different electrodes, particularly because quite low mass loadings often are used in many studies even though their capacities are too low to be of practical importance. Because the current used in the constant-current experiment depends linearly on the mass loading of the electroactive components, it is immediately evident that significantly larger *iR* drops and hence lower capacities will be seen upon using electrodes with higher mass loadings unless the increased *iR* drop is compensated for by an appropriate adjustment of the cut-off limits.

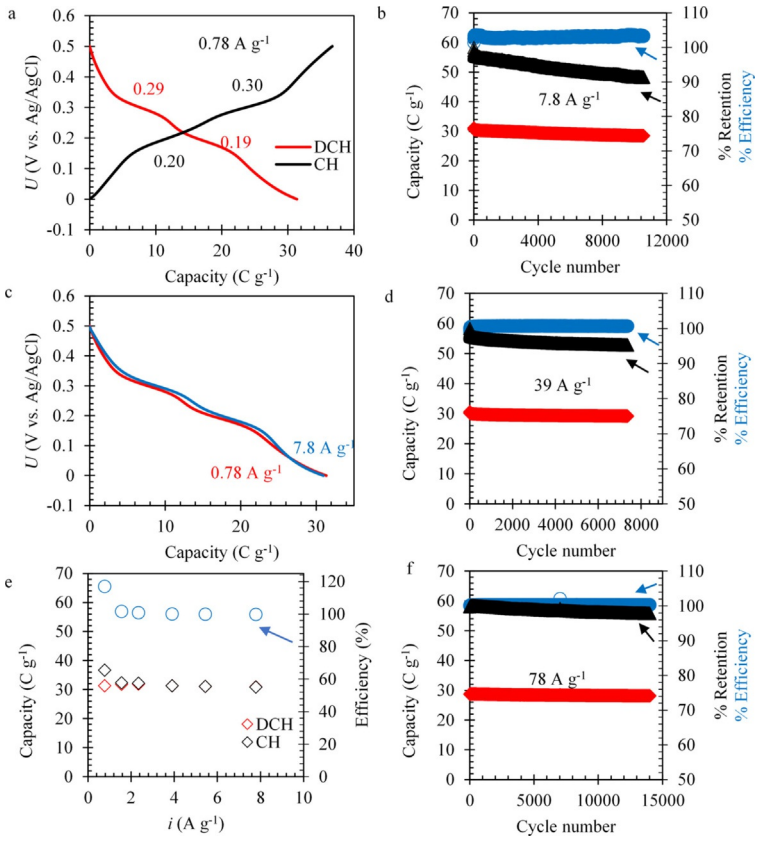

Figure 3. Electrochemical behavior of MoO_{3-x}–CNTs–CC paper electrodes under constant-current conditions. (a) Charge and discharge curves for a current density of 0.78 A g^{-1}. (c) Discharge profiles for current densities of 0.78 and 7.8 A g^{-1}. (e) Capacity and coulombic efficiency as a function of the current density. (b, d, f) Discharge capacity (red), capacity retention (black), and coulombic efficiency (blue) as a function of the cycle number, for current densities of 7.8, 39, and 78 A g^{-1}, respectively.

The MoO_{3-x}–CNTs–CC paper electrodes were also cycled for approximately 11 000 cycles with a current density 7.8 A g^{-1}. The capacity retention was approximately 91%, and the coulombic efficiency was approximately 100%, which indicates a high reversibility of the redox reaction and the absence of parasitic reactions (see Figure 3b). The observed small capacity loss can be attributed to the dissolution of the MoO_{3-x} in the electrolyte.[30,46,47] As seen in Figure 3d,f, the capacity retentions were approximately 95 and 97%, respectively, when the MoO_{3-x}–CNTs–CC electrode was further cycled for 8000 and 14 000 cycles at current densities of 39 and 78 A g^{-1}, respectively. These results indicate that the MoO_{3-x}–CNTs–CC paper electrode can be cycled over 30 000 cycles without a major capacity loss (see Figure S4 in the Supporting Information). In addition, the morphology of the MoO_{3-x}–CNTs–CC electrode remained almost unchanged after long-term cycling (see Figure S4c in the Supporting Information).

It was shown previously that the accessible capacity of the MoO_{3-x} nanosheets dropped significantly as the loading of the electrodes increased from 6.25 to 50 μg cm^{-2}.[28] For instance, when the loading was approximately 50 μg cm^{-2} (corresponding to a thickness of 8–11 μm), the capacity dropped to approximately 20 and 10 C g^{-1} at scan rates of 20 and 1000 mV s^{-1}, respectively. In the present study, we successfully increased the mass loading to approximately 0.9 mg cm^{-2} (corresponding to a thickness of approximately 12 μm) and achieved a capacity of approximately 30 C g^{-1} at scan rates of 20 or

1000 mV s^{-1}. Furthermore, the long-term cycling was previously limited to approximately 2000 cycles;[28] however, in this study we achieved a cycling stability over 30 000 cycles. These observations clearly prove that the immobilization of nanostructured MoO_{3-x} onto a 3D network of CNTs–CC fibers can successfully improve the accessible capacity, rate capability, and long-term cycling. Therefore, the accessible capacity of the MoO_{3-x}–CNTs–CC electrodes is not as promising compared with the theoretical one; however, it is superior compared with a previous study on the same material.[28] Table S2 (in the Supporting Information) includes a comparison of the performances of the present MoO_{3-x}–CNTs–CC electrodes as well as those of other MoO_3-based electrodes reported in the literature. Although it can be seen that this MoO_{3-x}–CNTs–CC electrode did not show a superior gravimetric capacity;[11,28,35,38] an excellent high-rate performance and long-term cycling stability were found for electrodes with a mass loading of approximately 0.9 mg cm^{-2}.

All in all, the excellent electrochemical stability and high-rate performance can be attributed to the high reversibility of the redox surface-confined reactions, homogeneous distribution of the oxide layer over the conductive nanofibril network, the absence of diffusion limitations, small increase in the *iR* drop upon increasing the current density owing to the low applied current (resulting from the relatively low mass loading), and the accommodated internal strain inside the flexible paper electrodes.[16,42] The specific gravimetric capacity can be improved by using 3 M H_2SO_4 solution, probably owing to lower *iR* drop and higher ionic conductivity (see Figure S5 in the Supporting Information). However, the capacity fading is highly pronounced, most likely as a result of dissolution of the oxide and degradation of the CNTs–CC network by the strongly oxidizing acidic electrolyte.[30,46,47] Further electrochemical and analytical studies are still needed to understand the electrochemical behavior of the MoO_{3-x}–CNTs–CC electrodes in 3 M H_2SO_4.

Conclusions

Flexible MoO_{3-x}–CNTs–CC (nanostructured MoO_{3-x} embedded in a carbon nanotube and *Cladophora* cellulose matrix) paper electrodes were prepared by using a straightforward and robust filtration-based method. SEM combined with energy-dispersive X-ray spectroscopy showed that the electrode thickness was approximately 12 μm and the molybdenum oxide was uniformly distributed within the CNTs–CC matrix. The MoO_{3-x}–CNTs–CC delivered a reversible capacity of 30 C g^{-1} at current densities between 0.78 and 78 A g^{-1}. The comparatively low capacity value suggested that only the surface layer of the oxide was electroactive. The long-term cycling of the electrodes shows that the electrodes can be cycled for more than 30 000 cycles without a major capacity loss or a drastic structural change in the active material.

The analysis of the peak currents and potentials for the redox peaks seen in the cyclic voltammetry showed that the electrode kinetics were fast, and that the polarization was mainly owing to the *iR* drop. The outstanding cyclability and rate capability of the MoO_{3-x}–CNTs–CC electrodes can be mainly attributed to four factors: (1) the surface-confined nature of the redox reaction, (2) absence of diffusion limitations, (3) high electronic conductivity and flexibility of the electrodes, and (4) the quite low increase in *iR* drop with the current density owing to the relatively low mass loading and lateral dimensions of the electrodes used in the electrochemical experiments.

Experimental Section

Preparation of the paper electrodes

The flexible freestanding electrodes were prepared according to the previously reported protocol,[23,24] with some modification as explained below. In a typical experiment, MoO_{3-x} nanosheet powder (70 mg, prepared as previously described),[28] multi-walled CNTs (20 mg), and *Cladophora* cellulose (10 mg) were added to a mixture containing water (60 mL) and ethanol (20 mL). The obtained mixture was subjected to sonication for 20 min by using high-energy ultrasonic equipment (Sonics and Materials Inc., USA, Vibra-Cell 750) under water cooling. The mixture was then drained through a polypropylene filter to form a filter cake and subsequently dried to form a paper sheet. The paper sheet could be directly used as a freestanding electrode with an active mass (mass of MoO_{3-x} and CNTs) loading of 0.9 mg cm^{-2}, and the overall electrode weight including the nanocellulose was approximately 1 mg cm^{-2}. Likewise, the CNT–CC paper electrodes were prepared by using a mixture of CNT and CC in 1:1 weight ratio.

Material characterization and electrochemical measurements

The morphology and elemental mapping of the electrodes were explored by SEM (LEO 1550 Gemini) equipped with an EDX detector. XRD measurements were performed by using a PANalytical diffractometer, equipped with CuK_α radiation ($\lambda = 1.54$ Å). The Young's modulus for the MoO_{3-x}–CNTs–CC paper was obtained from nanoindentation tests by using a Hysitron Ti950 triboindentor device equipped with a Berkovich indenter. An array of 3×3 indentations with a trapezoidal loading profile was used together with a 1000 μN peak load. A standard fused silica was used for calibrating the instrument prior the measurements. The electronic conductivity of the MoO_{3-x}–CNTs–CC paper was determined by using a Jandel Four Point Probe system (with a 0.63 mm probe spacing).

All electrochemical measurements were performed in a three-electrode configuration by using a stainless-steel Swagelok cell with activated carbon (YP-50, Kuraray, Japan) as the counter electrode and Ag/AgCl (1 M KCl) reference electrodes. The MoO_{3-x}–CNTs–CC electrodes used as the working electrodes were placed on a gold foil current collector. A piece of Celgard 3501 soaked in 1 M H_2SO_4 was used as the separator. The overall working electrode mass varied between 100 and 210 μg, and the capacities were normalized with respect to the mass of the redox-active materials, the mass of MoO_{3-x} and CNTs. The electrodes' lateral dimensions were approximately 2–3 mm. A few experiments were performed by using electrodes of dimension 5 mm×7 mm and mass loading of 320 μg. CV and constant-current techniques were used to study the electrochemical behavior of the electrodes in the potential window between 0 and 0.5 V vs. Ag/AgCl (1 M KCl). For the experiments with CNTs–CC electrodes, the overall working electrode mass was approximately 180 μg (2–3 mm lateral dimensions), and the capacities were normalized with respect to the mass of CNTs, that is, 50% of total electrode mass.

Acknowledgements

J.R. acknowledges support from the Swedish Foundation for Strategic Research (SSF) for Project Funding (EM16-0004) and the Knut and Alice Wallenberg (KAW) Foundation for a fellowship grant and project funding (KAW 2015.0043).

Conflict of interest

The authors declare no conflict of interest.

Keywords: carbon nanotubes · charge storage applications · *Cladophora* cellulose · molybdenum oxide · paper electrodes

[1] M. Winter, R. J. Brodd, *Chem. Rev.* **2004**, *104*, 4245.
[2] M. S. Whittingham, *Chem. Rev.* **2004**, *104*, 4271.
[3] N. Yabuuchi, K. Kubota, M. Dahbi, S. Komaba, *Chem. Rev.* **2014**, *114*, 11636.
[4] B. E. Conway, *Electrochemical Supercapacitors: Scientific Fundamentals and Technological Applications*, Springer US, Boston, MA, **1999**.
[5] E. Frackowiak, Q. Abbas, F. Béguin, *J. Energy Chem.* **2013**, *22*, 226.
[6] F. Béguin, V. Presser, A. Balducci, E. Frackowiak, *Adv. Mater.* **2014**, *26*, 2219.
[7] X. Zhao, B. M. Sánchez, P. J. Dobson, P. S. Grant, *Nanoscale* **2011**, *3*, 839.
[8] S. D. Perera, B. Patel, N. Nijem, K. Roodenko, O. Seitz, J. P. Ferraris, Y. J. Chabal, K. J. Balkus, *Adv. Energy Mater.* **2011**, *1*, 936.
[9] X. Rui, Z. Lu, Z. Yin, D. H. Sim, N. Xiao, T. M. Lim, H. H. Hng, H. Zhang, Q. Yan, *Small* **2013**, *9*, 716.
[10] L. Nyholm, G. Nyström, A. Mihranyan, M. Strømme, *Adv. Mater.* **2011**, *23*, 3751.
[11] K. Zhou, W. Zhou, X. Liu, Y. Sang, S. Ji, W. Li, J. Lu, L. Li, W. Niu, H. Liu, S. Chen, *Nano Energy* **2015**, *12*, 510.
[12] O. Nechyporchuk, M. N. Belgacem, J. Bras, *Ind. Crops Prod.* **2016**, *93*, 2.
[13] J. Shojaeiarani, D. Bajwa, A. Shirzadifar, *Carbohydr. Polym.* **2019**, *216*, 247.
[14] J. Wang, J. Tavakoli, Y. Tang, *Carbohydr. Polym.* **2019**, *219*, 63.
[15] S. Zhou, L. Nyholm, M. Strømme, Z. Wang, *Acc. Chem. Res.* **2019**, *52*, 2232.
[16] Z. Wang, P. Tammela, M. Strømme, L. Nyholm, *Adv. Energy Mater.* **2017**, *7*, 1700130.
[17] D. Tobjörk, R. Österbacka, *Adv. Mater.* **2011**, *23*, 1935.
[18] L. Yuan, X. Xiao, T. Ding, J. Zhong, X. Zhang, Y. Shen, B. Hu, Y. Huang, J. Zhou, Z. L. Wang, *Angew. Chem. Int. Ed.* **2012**, *51*, 4934; *Angew. Chem.* **2012**, *124*, 5018.
[19] A. Razaq, L. Nyholm, M. Sjödin, M. Strømme, A. Mihranyan, *Adv. Energy Mater.* **2012**, *2*, 445.
[20] G. Nyström, A. Razaq, M. Strømme, L. Nyholm, A. Mihranyan, *Nano Lett.* **2009**, *9*, 3635.
[21] H. Olsson, G. Nyström, M. Strømme, M. Sjödin, L. Nyholm, *Electrochem. Commun.* **2011**, *13*, 869.
[22] B. Yao, J. Zhang, T. Kou, Y. Song, T. Liu, Y. Li, *Adv. Sci.* **2017**, *4*, 1700107.
[23] Z. Wang, C. Xu, P. Tammela, P. Zhang, K. Edström, T. Gustafsson, M. Strømme, L. Nyholm, *Energy Technol.* **2015**, *3*, 563.
[24] Z. Wang, C. Xu, P. Tammela, J. Huo, M. Strømme, K. Edström, T. Gustafsson, L. Nyholm, *J. Mater. Chem. A* **2015**, *3*, 14109.
[25] A. S. Etman, A. J. Pell, P. Svedlindh, N. Hedin, X. Zou, J. Sun, D. Bernin, *ACS Omega* **2019**, *4*, 10899.
[26] A. S. Etman, A. K. Inge, X. Jiaru, R. Younesi, K. Edström, J. Sun, *Electrochim. Acta* **2017**, *252*, 254.
[27] A. S. Etman, J. Sun, R. Younesi, *J. Energy Chem.* **2019**, *30*, 145.
[28] A. S. Etman, L. Wang, K. Edström, L. Nyholm, J. Sun, *Adv. Funct. Mater.* **2019**, *29*, 1806699.
[29] A. S. Etman, H. N. Abdelhamid, Y. Yuan, L. Wang, X. Zou, J. Sun, *ACS Omega* **2018**, *3*, 2193.
[30] V. S. Saji, C.-W. Lee, *ChemSusChem* **2012**, *5*, 1146.
[31] X. Zhang, C. Fu, J. Li, C. Yao, T. Lu, L. Pan, *Ceram. Int.* **2016**, *43*, 3769.
[32] L. S. Aravinda, U. Bhat, B. Ramachandra Bhat, *Electrochim. Acta* **2013**, *112*, 663.
[33] I. Shakir, M. Sarfraz, *Electrochim. Acta* **2014**, *147*, 380.
[34] D. Hanlon, C. Backes, T. M. Higgins, M. Hughes, A. O'Neill, P. King, N. McEvoy, G. S. Duesberg, B. Mendoza Sanchez, H. Pettersson, V. Nicolosi, J. N. Coleman, *Chem. Mater.* **2014**, *26*, 1751.
[35] B. Yao, L. Huang, J. Zhang, X. Gao, J. Wu, Y. Cheng, X. Xiao, B. Wang, Y. Li, J. Zhou, *Adv. Mater.* **2016**, *28*, 6353.
[36] S. H. Yu, S. H. Lee, D. J. Lee, Y. E. Sung, T. Hyeon, *Small* **2016**, *12*, 2146.
[37] H.-S. Kim, J. B. Cook, H. Lin, J. S. Ko, S. H. Tolbert, V. Ozolins, B. Dunn, *Nat. Mater.* **2017**, *16*, 454.
[38] T. Li, M. Beidaghi, X. Xiao, L. Huang, Z. Hu, W. Sun, X. Chen, Y. Gogotsi, J. Zhou, *Nano Energy* **2016**, *26*, 100.
[39] L. Huang, B. Yao, J. Sun, X. Gao, J. Wu, J. Wan, T. Li, Z. Hu, J. Zhou, *J. Mater. Chem. A* **2017**, *5*, 2897.
[40] A. S. Etman, *Aqueous Exfoliation of Transition Metal Oxides for Energy Storage and Photocatalysis Applications: Vanadium Oxide and Molybdenum Oxide Nanosheets*, PhD Thesis, Stockholm University (Sweden), **2019**.
[41] J. Zhou, J. Song, H. Li, X. Feng, Z. Huang, S. Chen, Y. Ma, L. Wang, X. Yan, *New J. Chem.* **2015**, *39*, 8780.
[42] Z. Wang, X. Zhang, S. Zhou, K. Edström, M. Strømme, L. Nyholm, *Adv. Funct. Mater.* **2018**, *28*, 1804038.
[43] N. Anbananthan, K. Nagaraja Rao, V. K. Venkatesan, *J. Electroanal. Chem.* **1994**, *374*, 207.
[44] B. Mendoza-Sánchez, T. Brousse, C. Ramirez-Castro, V. Nicolosi, P. S. Grant, *Electrochim. Acta* **2013**, *91*, 253.
[45] A. Bard, L. Faulkner, *Electrochemical Methods: Fundamentals and Applications*, Wiley, Hoboken, **2001**.
[46] I. A. de Castro, R. S. Datta, J. Z. Ou, A. Castellanos-Gomez, S. Sriram, T. Daeneke, K. Kalantar-zadeh, *Adv. Mater.* **2017**, *29*, 1701619.
[47] M. Pourbaix, *Atlas of Electrochemical Equilibria in Aqueous Solutions*, Pergamon Press, Oxford, **1966**.

Manuscript received: September 2, 2019
Revised manuscript received: October 3, 2019
Accepted manuscript online: October 15, 2019
Version of record online: November 8, 2019